Environmental Science Nano

Synergistic Effects of Iron Oxide Nanoparticles and Hydrogen Peroxide in Inhibiting Pseudomonas aeruginosa Growth to Combat Bacterial Contamination in Water Recovery Systems

Journal:	*Environmental Science: Nano*
Manuscript ID	EN-ART-12-2024-001164.R1
Article Type:	Paper

Environmental Significance Statement

This study addresses critical environmental challenges associated with water treatment by demonstrating the use of iron oxide nanoparticles (IONPs), both bare and polyacrylic acid-coated (PAA@IONPs), to enhance the effectiveness of hydrogen peroxide in controlling Pseudomonas aeruginosa in water systems. By potentially reducing the required concentrations of hydrogen peroxide, this approach minimizes the environmental and toxicological impacts of biocides commonly used in water treatment. The successful application of nanotechnology in reducing biocide levels offers significant implications for improving water quality and safety, aligning with environmental goals of reducing chemical usage while effectively managing bacterial pathogens in water resources. This innovation represents a substantial advancement in the field of environmental science, emphasizing the role of nanoscale materials in sustainable water management practices.

Synergistic Effects of Iron Oxide Nanoparticles and Hydrogen Peroxide in Inhibiting *Pseudomonas aeruginosa* Growth to Combat Bacterial Contamination in Water Recovery Systems

Omid Sedighi[1], Tucker Johnsen[1], Appala Raju Badireddy[2], Matthew J. Wargo[3], Amber L. Doiron[1]*

[1]Department of Electrical and Biomedical Engineering, University of Vermont, VT, USA
[2]Department of Civil and Environmental Engineering, University of Vermont, VT, USA
[3]Department of Microbiology and Molecular Genetics, University of Vermont, VT, USA

*Correspondence should be addressed to Amber Doiron via email: amber.doiron@uvm.edu
Address: 33 Colchester Ave. Burlington, VT 05405

Abstract:

Access to safe water is critical for public health. *Pseudomonas aeruginosa* is ranked as one of the most significant bacterial pathogens, threatening human health. Hydrogen peroxide and other biocides are often used to prevent the growth of bacteria, but the toxicity of these biocides is a major consideration when bacteria grow in water sources. This study explores the application of iron oxide nanoparticles (IONPs), both bare and polyacrylic acid-coated (PAA@IONPs), to enhance the effectiveness of hydrogen peroxide in eliminating *P. aeruginosa*, potentially reducing the required biocide concentrations and minimizing toxicity. X-ray diffraction crystallography (XRD) alongside X-Ray photoelectron spectroscopy (XPS) showed that the synthesized IONPs were magnetite nanoparticles and Fourier-transform infrared (FTIR) spectroscopy proved that PAA coating was successfully functionalized to IONPs. The hydrodynamic size of the IONPs decreased from 106 ± 11 nm to 84 ± 3 nm when coated with PAA. Transmission electron microscopy (TEM) images confirmed a similar decrease in dry size from 16 ± 3 nm to 9 ± 2 nm post-coating. A week after storage, there was a decrease in the concentration of stored IONPs and PAA@IONPs due to settling by 56

± 14% and 22.6 ± 0.6%, respectively, demonstrating that PAA coating increased colloidal stability of the IONPs. Coated nanoparticles exhibited a more negative zeta potential, which was also indicative of greater colloidal stability. In the presence of 3.65 mg/ml IONPs and 182.25 mM of hydrogen peroxide, overnight bacterial growth was reduced by more than 63% compared to the sample with hydrogen peroxide alone. IONPs did not inhibit bacterial growth in the absence of hydrogen peroxide. Presence of 3.65 mg/ml IONPs and 182.25 mM of hydrogen peroxide killed 90.2% of bacterial cells during one hour of exposure. These findings indicate the potential benefit of IONPs to combat bacterial growth, which could be applied in industrial settings to reduce the biocide concentration needed to curb bacterial development.

Keywords: magnetite nanoparticles, Polyacrylic acid, *Pseudomonas aeruginosa*, antibacterial, hydrogen peroxide, spot serial dilution.

Introduction:

Safe and available water is vital for public health whether consumed for drinking, domestic use, food production, or recreational purposes. According to world health organization (WHO), microbiologically contaminated water results in around 505,000 diarrheal deaths annually [1]. *Pseudomonads* are highly adaptable bacteria capable of thriving in diverse environments, including distilled water, and they have been linked to outbreaks through contaminated recreational and tap water [2]. *Pseudomonas aeruginosa* is a prevalent, mobile, non-fermentative, Gram–negative bacterium and an opportunistic pathogen categorized as an ESKAPE pathogen [3, 4] . The ability of *P. aeruginosa* to form biofilms in an aqueous environment makes the traditional treatment methods even less effective. Therefore, there is an ongoing need to develop new technologies to kill these bacteria and inhibit their growth more efficiently to prevent human disease.

Biocides are chemical agents with antimicrobial properties extensively used in homes, industries, and healthcare settings for disinfection purposes [5]. Hydrogen peroxide (H_2O_2) is a non-radical reactive oxygen species (ROS) that acts as a biocide and effectively kills bacterial cells. Hydrogen peroxide damages vital cellular components like DNA, proteins, and cell membranes, disrupting critical biological processes and leading to bacterial cell death [6, 7]. However, high concentrations of hydrogen peroxide in water resources can cause toxicity [8]. Drinking hydrogen peroxide at concentrations higher than 3% (equivalent to 880mM) is toxic to humans. Even at lower concentrations, prolonged consumption of hydrogen peroxide can lead to toxicity [9]. Therefore, it is crucial to minimize the presence of hydrogen peroxide in water resources as much as possible. Iron oxide nanoparticles (IONPs) can enhance the efficiency of hydrogen peroxide in generating radical ROS through a reaction known as the Fenton and Fenton-like reactions [10]. During these reactions, hydrogen peroxide is converted to hydroxyl radicals ($OH^{\cdot}$) in the presence of iron (Fe^{2+}, and Fe^{3+}) (equation 1 and 2) [11]. This reaction is important because the products of the decomposition of hydrogen peroxide (hydroxyl radical and peroxide radical) are more potent than non-radical H_2O_2. These radicals are highly reactive and increase oxidative stress in bacterial cells more efficiently than hydrogen peroxide alone [12, 13].

$$Fe^{2+} + H_2O_2 \rightarrow Fe^{3+} + OH^{\cdot} + OH^{-} \quad \text{(Equation 1)}$$

$$Fe^{3+} + H_2O_2 \rightarrow Fe^{2+} + HO_2^{\cdot} + H^{+} \quad \text{(Equation 2)}$$

Even though IONPs have been utilized in water treatment as a means of killing bacteria through hyperthermia [14, 15] or delivery of pharmaceutics [16], the

particles themselves do not exhibit antibacterial activity [17]. IONPs are non-toxic and magnetic, enabling most of their applications in biomedicine [18]. Here we studied the impact of addition of IONPs and PAA@IONPs to hydrogen peroxide in order to inhibit bacterial growth and kill the already existing bacterial cells. Based on the literature, IONPs should be able to increase antibacterial properties of hydrogen peroxide by production of hydroxyl radicals.

IONPs exist in several oxidation states, with the three most frequent forms of magnetite (Fe_3O_4), maghemite (γ-Fe_2O_3), and hematite (α-Fe_2O_3). The oxidation state of the synthesized IONPs, is crucial since magnetite contains both Fe(II) and Fe(III) ions and can effectively catalyze the Fenton reaction, while maghemite, and hematite predominantly contain Fe(III) ions. As shown in Equations 1 and 2, the final products of reactions can differ depending on whether Fe(II) or Fe(III) is present. Hydroxyl radicals are produced when Fe(II) reacts with hydrogen peroxide, while superoxide anions are generated in the presence of Fe(III). The key difference is that the hydroxyl radical is a stronger ROS agent and is therefore preferred [19]. This underscores the importance of controlling the oxidation state of IONPs during synthesis. The size-dependence of the magnetic and catalysis properties of IONPs demands precise control over the synthesis process. A challenge with IONPs is their tendency to aggregate, which negatively impacts their magnetic characteristics and colloidal stability. To enhance the colloidal stability of IONPs, a polymeric coating was applied. Among the various polymeric coatings available, PAA was selected due to its dual benefits. Firstly, due to literature PAA-coated IONPs exhibit improved antibacterial properties, making them advantageous for our applications. Secondly, PAA enhances biocompatibility, ensuring that the modified IONPs maintain low cytotoxicity to human cells [20]. This combination of stability, antimicrobial activity, and biocompatibility makes PAA an optimal choice for functionalizing IONPs. Numerous studies have investigated the antibacterial properties of IONPs and hydrogen peroxide. Additionally, the Fenton reaction has been extensively explored for various applications, including cancer therapy and water treatment [21, 22]. However, to the best of our knowledge, there is no comprehensive study specifically examining the use of IONPs to enhance antibacterial efficacy of hydrogen peroxide against *Pseudomonas aeruginosa* in water resources. This study demonstrates the synergistic antibacterial effects of PAA@IONPs, IONPs, and hydrogen peroxide against *P. aeruginosa*. Additionally, we reassessed the impact of PAA coating on IONPs, focusing on its influence on antibacterial properties and nanoparticle stability. Our results indicate that with the

assistance of IONPs, the minimum hydrogen peroxide concentration required to eliminate bacteria can be reduced to 182.25 mM, a level below the threshold for hydrogen peroxide toxicity [23]. Furthermore, since iron oxide nanoparticles can be collected using a magnetic field, they can be efficiently separated from the water source, preventing secondary exposure. We believe this method offers a safe and effective approach for bacterial eradication in water recovery systems, particularly in space missions, where access to clean water is extremely limited.

Materials and Methods

1- Materials

Iron (II) chloride ($FeCl_2$), iron (III) chloride ($FeCl_3$), ammonium hydroxide (NH_4OH, 28.0-30.0% NH_3 basis), silicone oil, polyacrylic acid (PAA) (M_w = 72.06 g/mol), hydrogen peroxide solution (H_2O_2), and potassium chloride (KCl) were purchased from Sigma-Aldrich (St. Louis, MO, USA). Tryptic Soy Broth was purchased from MP Biomedicals (CA, USA), and agar was purchased from Becton, Dickinson and Company (BD, NJ, USA). Ultrafiltered water was produced by Milli-Q Millipore Integral 10 water purification system. Nitrogen gas was from Airgas Inc. *P. aeruginosa* (PAO1) is Wargo Lab strain MJ79 derived from PAO1-W (PMID 10984043).

2- Synthesis of PAA Coated and Bare IONPs

IONPs were synthesized using a co-precipitation method (Figure 1) based on previously published protocols [24-26]. Throughout the synthesis procedure, nitrogen-purged ultrapure water (N_2/H_2O) was utilized to prevent oxidation. Separate solutions of iron (II) chloride (1 mmol) and iron (III) chloride (2 mmol) were prepared by dissolving each in 50 ml of N_2/H_2O. Once dissolved, the solutions were transferred to a filter flask under continuous nitrogen to keep the oxygen out. The solutions of iron chloride were combined and heated to 80°C in a silicone oil bath while being stirred at 600 RPM using a 2.5 cm magnetic stirrer on a hot plate stirrer (Thermo Fisher Scientific, Isotemp, USA). Then, 30 ml of 1 M aqueous ammonium hydroxide was introduced at the rate of 4.25 mmol/min using a syringe pump (NE-1000, New Era Pump Systems Inc., USA). After the ammonium hydroxide was completely added, the reaction mixture was allowed to proceed for 30 min, removed from heat, and cooled to room temperature. It was then sonicated for 30 min using an ultrasonic cleaner (VWR Symphony, Model: 97043-960, USA). The particles were washed and magnetically separated by decantation using a strong magnet (DY06, 2-inch diameter X 3/8-inch thickness, K&J Magnetics, Inc., PA, USA). This particle separation ensured separation of IONPs from unreacted dissolved constituents. Each particle batch was then re-suspended in 50 ml of

N_2/H_2O and sonicated for an extra 10 min. This was repeated three times until the pH stabilized at 6.5-7.5 or they were stable enough that could not be separated with the magnet anymore. For polyacrylic acid-coated iron oxide nanoparticles (PAA@IONPs), PAA (25% w/w with respect to the Fe(II) salt) was added to the reaction medium just before the addition of ammonium hydroxide. Due to the high stability of coated particles, they were washed by centrifuging at 55,000 ×g for 20 min. Finally, the pellet was separated and suspended in N_2/H_2O until the final volume of 50 ml was achieved.

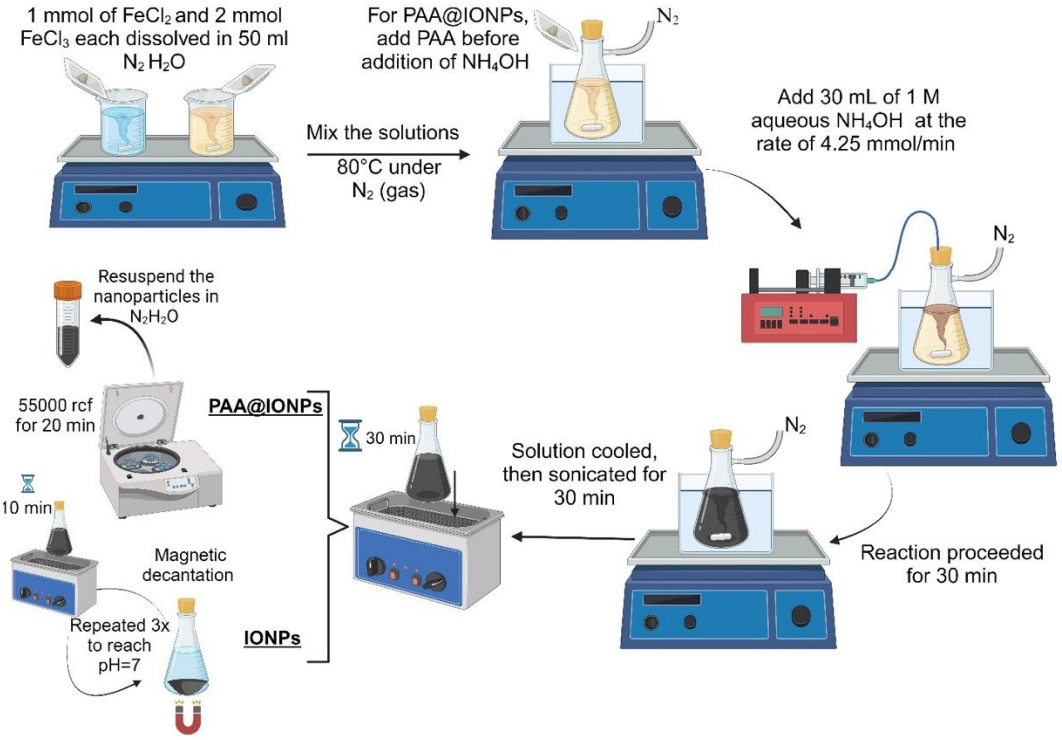

Figure 1 Schematic of synthesis of IONPs (Created with BioRender.com)

3- Material Characterization

The crystallographic structure of bare and PAA@IONPs was characterized by powder X-ray diffraction crystallography (XRD, Rigaku Miniflex II, equipped with a Cu X-ray tube, Rigaku Corporation, Japan). XRD was operated using a 2theta-theta geometry over a 2q range from 10° to 70° with a 1°/min dwelling time. The results were then analyzed using a profile fitting module within the PDXL-2 software (Rigaku Corp., Japan). To detect the functional groups on the surface of coated and bare IONPs, Fourier-transform infrared spectroscopy (FTIR, Nicolet™ iS50 FTIR Spectrometer, Thermo Scientific, USA) was used. The elemental composition and oxidation states of the nanoparticles' surface were investigated by X-ray photoelectron spectroscopy spectra (XPS, The Kratos Axis Supra XPS, UK).

Nanoparticle size was determined using two different techniques. First, the hydrodynamic size of nanoparticles was measured using nanoparticle tracking analysis (NTA, Zetaview Twin PMX-110, Particle Metrix GmbH, Germany). For NTA, the samples were sonicated for 10 min to achieve thorough dispersion before analysis and were introduced into the flow chamber at a concentration of 0.4 mg/ml at room temperature using a disposable syringe. To account for the repeatability of our study, NTA was conducted on five (shown as n) different synthesized batches of nanoparticles. Next, the dry size and shape were studied using transmission electron microscopy (TEM, JEOL JEM-1400, JEOL Ltd., Japan) at an acceleration voltage of 80 kV. TEM samples were prepared by diluting the nanoparticle suspension to 0.4 mg/ml and depositing a drop onto a 100-mesh nickel grid backed by a carbon support film (LADD Research Industries, USA), which was left to air dry overnight. The polydispersity index (PdI) and zeta potential of the nanoparticles were determined using dynamic and electrophoretic light scattering (DLS, Zetasizer NanoZSP, Malvern Panalytical Inc., UK). For this purpose, samples were diluted in 10 mM KCl and added to DTS1070 folded capillary cell for analysis. To quantify the number of suspended nanoparticles, two aqueous solutions were prepared in triplicate: one containing 0.4 mg/ml of IONPs and the other containing 0.4 mg/ml of PAA@IONPs. All samples were then sonicated for 10 min. Post-sonication, the samples were left undisturbed for our storage study. At each time interval, three 200 µl aliquots were taken from the samples, transferred to a 96-well plate, and analyzed using a UV-vis spectrophotometer (SpectraMax i3x, Molecular Devices, USA). For this study, three samples of each IONPs and PAA@IONPs were prepared, and from each sample, triplicates (shown as n) were aliquoted for analysis.

4- Bacterial Growth Studies

During this study, *P. aeruginosa* PAO1 was streaked onto tryptic soy agar (TSA) from glycerol stocks stored at -80°C and incubated for 15 h at 37°C. First, we assessed the impact of various hydrogen peroxide concentrations on *P. aeruginosa* in the absence of nanoparticles. *P. aeruginosa* cultures were exposed to different concentrations of hydrogen peroxide and bacterial growth was measured to determine the minimal concentration of hydrogen peroxide that robustly reduced bacterial growth without completely inhibiting it. Dilutions of hydrogen peroxide were prepared in three serial sets: 2000, 400, 80, 16, and 3.2 mM; 182.25, 121.5, 81, 54, 36, and 24 mM; and 16, 8, 4, 2, 1, 0.5 mM. The effect of this biocide on bacterial growth was measured by the net growth, which is defined as the difference in optical density at 600 nm (OD_{600}) observed 12 h after incubation compared to before incubation, using a UV-vis spectrophotometer.

In the next step, the impact of coated and bare IONPs on *P. aeruginosa* was measured. We hypothesized that the presence of IONPs alongside hydrogen peroxide would initiate the Fenton and Fenton-like reactions, leading to greater bacterial growth inhibition compared to scenarios without IONPs. To test the hypothesis, a colony of *P. aeruginosa* was transferred into 3 ml of TSB media and incubated overnight at 37°C. To prepare the seed cultures the incubated bacteria was diluted to $OD_{600}= 0.05 \pm 0.01$. This dilution was necessary for the subsequent growth study to standardize the starting bacterial concentration, ensuring consistency and reliability in our experimental results. Meanwhile, six samples each of PAA@IONPs and IONPs were prepared, starting at a concentration of 3.65 mg/ml, and serially diluted in water in a 1:2 ratio until a final dilution of 1:32 was achieved. Hydrogen peroxide (182.25 mM) was added to the seed culture to achieve a total volume of 50 ml for further studies. This solution was added to each well of a 24 well-plate and then 10 µl of various concentrations of IONPs or PAA@IONPs were added to the wells to reach a final volume of 1 ml in each well. Each experiment was conducted in triplicate.

One indicator of a Fenton-like reaction is the change in the pH of the solution due to H^+ generation. To investigate this, IONPs and PAA@IONPs were added to two solutions: TSB and TSB+182.25 mM H_2O_2. The concentrations used were the same as those in the bacterial growth inhibition study, and all samples were prepared in triplicate. The pH of the solutions was measured immediately after adding the nanoparticles using a pH meter (Fisherbrand™ accumet™ AB150 pH Benchtop Meters, USA). All samples were then incubated at 37°C for 12 h, followed by another pH measurement

To compare the effects of nanoparticles and biocide treatments on bacterial growth, control experiments were carried out without nanoparticles and hydrogen peroxide as well as hydrogen peroxide without nanoparticles. In all studies, a blank sample of TSB alone was included to ensure there was no contamination.

5- Antibacterial Study

A spot serial dilution method was used to study the antibacterial properties of the biocide hydrogen peroxide and IONPs. Briefly, the bacterial culture was grown over night in TSB and then diluted with TSB to achieve an OD_{600} of 0.1 to start the study. Five samples were prepared including a blank of TSB alone, bacteria in TSB, H_2O_2 and bacteria, IONPs and H_2O_2 with bacteria, and PAA@IONPs and H_2O_2 with bacteria. Each sample had an initial volume of 1 ml. The concentration of H_2O_2 in all samples was 182.25 mM, and the samples containing nanoparticles had 10 µl of nanoparticles at a concentration of 3.65 mg/ml. After thorough mixture, 200 µl of

each sample was transferred to a 96-well plate in triplicate. Serial dilutions in TSB were then performed for all samples, with a 10-fold dilution until a dilution factor of 10^7 was achieved. Samples were incubated for an hour at 37°C, followed by the culture of 5 µl from each sample on tryptic soy agar, which was then incubated for 15 h. The colony development pattern at different dilutions was recorded as too many to read (tmtr), countable (6-30 range), no colony is formed (N/A). After recording the colony number, colony forming units (CFU) / 200 µl of samples was calculated by multiplying colony number by dilution factor.

All data were analyzed using a one-way ANOVA followed by Tukey's post-hoc t-test for statistical analysis, using p-value < 0.05 to determine statistical significance between means. GraphPad Prism version 10.2.2 (USA) was utilized for all statistical analyses.

Results:

1- XRD confirmed synthesis of IONPs

To investigate the crystal structure of the synthesized magnetic nanoparticles, X-ray diffraction (XRD) was performed on the coated and bare IONPs (Figure 2a). The XRD pattern of magnetite contained six strong peaks at $2\theta = 30.3°, 35.5°, 43.2°, 53.5°, 57.1°,$ and $62.9°$, which corresponded to (220), (311), (400), (422), (511), and (440) crystalline planes of IONPs, respectively (International Center for Diffraction Data PDF-19-0629) [27]. These six strong peaks can be observed in Figure 2a. The coating process did not alter peak positions, indicating preserved crystallinity. The coated samples showed lower intensity compared to bare IONPs, suggesting reduced XRD signal due to the presence of PAA [28].

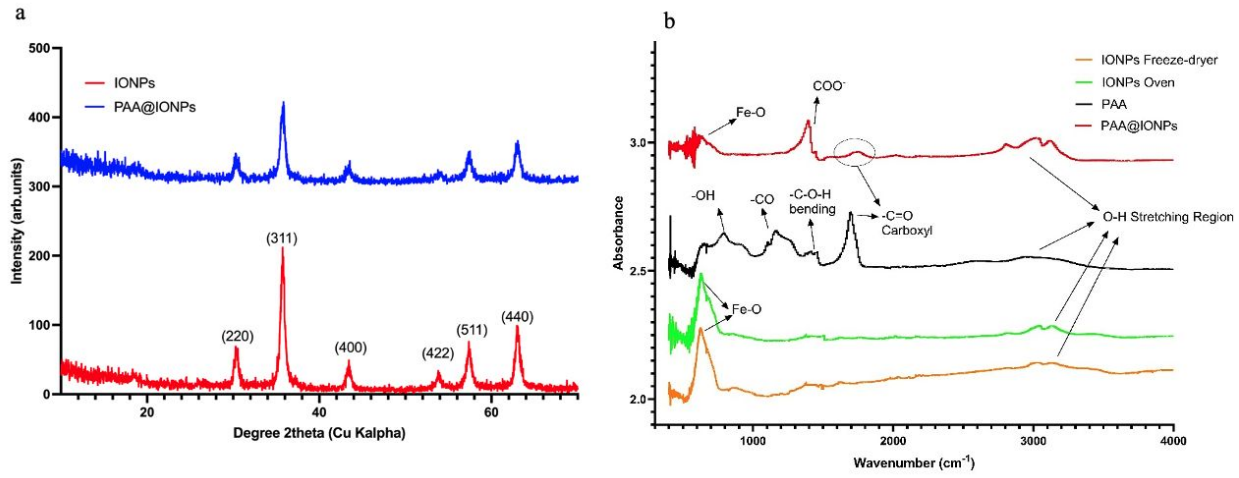

Figure 2 a) XRD peaks of IONPs and PAA@IONPs b) FTIR spectra of IONPs dried in freeze-dryer, IONPs dried in oven, PAA, and PAA@IONPs dried in oven

2- FTIR indicated bonding between iron and PAA

The FTIR spectra of the synthesized IONPs and PAA@IONPs are displayed in Figure 2b. FTIR spectra confirmed the presence of Fe–O vibrations at ~610 cm^{-1} in all samples, indicating iron oxide formation. A broad band between 3200–3500 cm^{-1} suggested adsorbed –OH groups, with higher intensity observed in oven-dried samples. The presence of a strong C=O peak at 1718 cm^{-1} in PAA diminished in PAA@IONPs, with the appearance of a COO^- peak at 1410 cm^{-1}, suggesting successful surface bonding between PAA and IONPs [29-31].

3- XPS revealed synthesis of magnetite nanoparticles

Due to sharing a spinal structure, Fe_3O_4 (magnetite), and γ-Fe_2O_3 can show similar XRD patterns; therefore, running XRD alone is not the most comprehensive way to distinguish these specific crystalline forms of IONPs. PAA@IONPs could not be effectively dried using a freeze-dryer; thus, oven drying was necessary. To distinguish Fe_3O_4 from γ-Fe_2O_3, XPS analysis was performed (Figure 3). The Fe 2p3/2 and Fe 2p1/2 peaks were observed at 711.1 eV and 724.3 eV, confirming Fe_3O_4 as the dominant phase [32]. A satellite peak at 718.5 eV, associated with γ-Fe_2O_3, was detected exclusively in oven-dried samples, suggesting oxidation occurred during drying rather than synthesis [33-35]. C 1s and O 1s peaks for the samples are shown and discussed in the supplementary materials. Briefly, the low intensity of the C=O peaks compared to the high-intensity C-O peak in the coated sample provides additional evidence of the chemical binding discussed in the FTIR data.

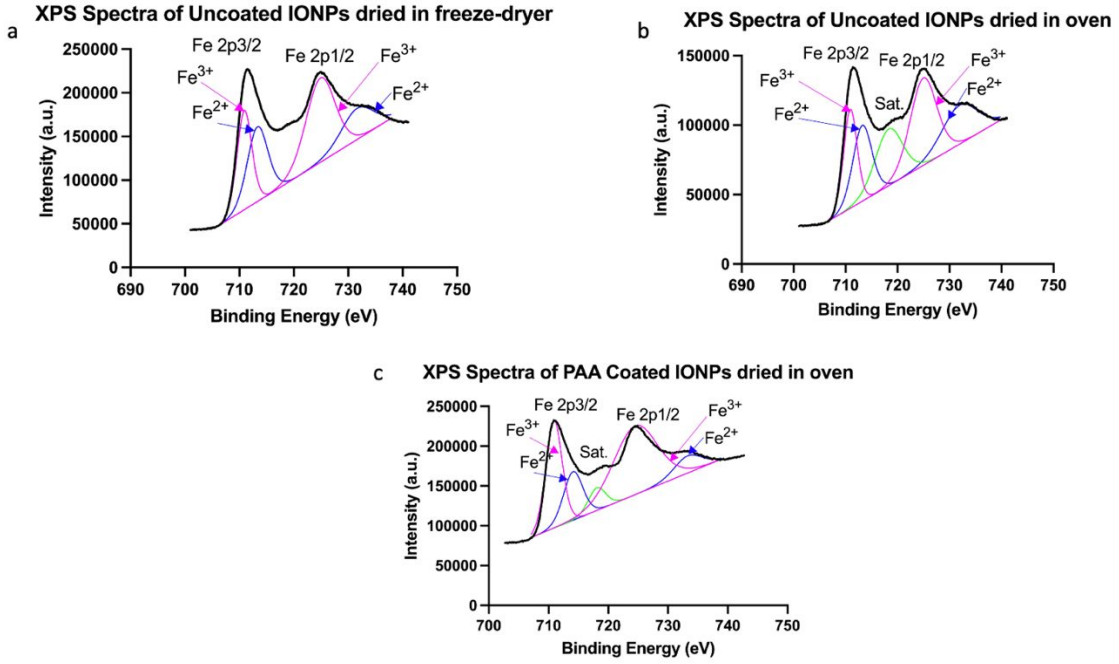

Figure 3 XPS analysis, Fe 2p XPS spectra of (a) IONPs dried in freeze-dryer (b) IONPs dried in oven (c) PAA@IONPs dried in oven.

4- TEM revealed spherical morphology and smaller IONPs when coated

TEM images revealed the morphology of synthesized nanoparticles and allowed for the measurement of their dry particle size, referred to as "dry size" in this analysis. Both IONPs and PAA@IONPs were predominantly spherical in shape. The mean size for the uncoated IONPs was 16 ± 3 nm, which was reduced to 9 ± 2 nm for PAA@IONPs. As seen in the histograms (Figure 4c,d), in both cases the distribution of size was close to normal with no great outliers. The bar graph (Figure 4e) depicts a comparison of coated and uncoated IONPs, where each bar represents the mean value of dry sizes, with error bars indicating the standard deviation for each group. The uncoated samples showed a significantly higher mean value compared to the coated particles. Running a t-test on the samples provides further evidence of a statistically significant impact of coating on the dry size of IONPs.

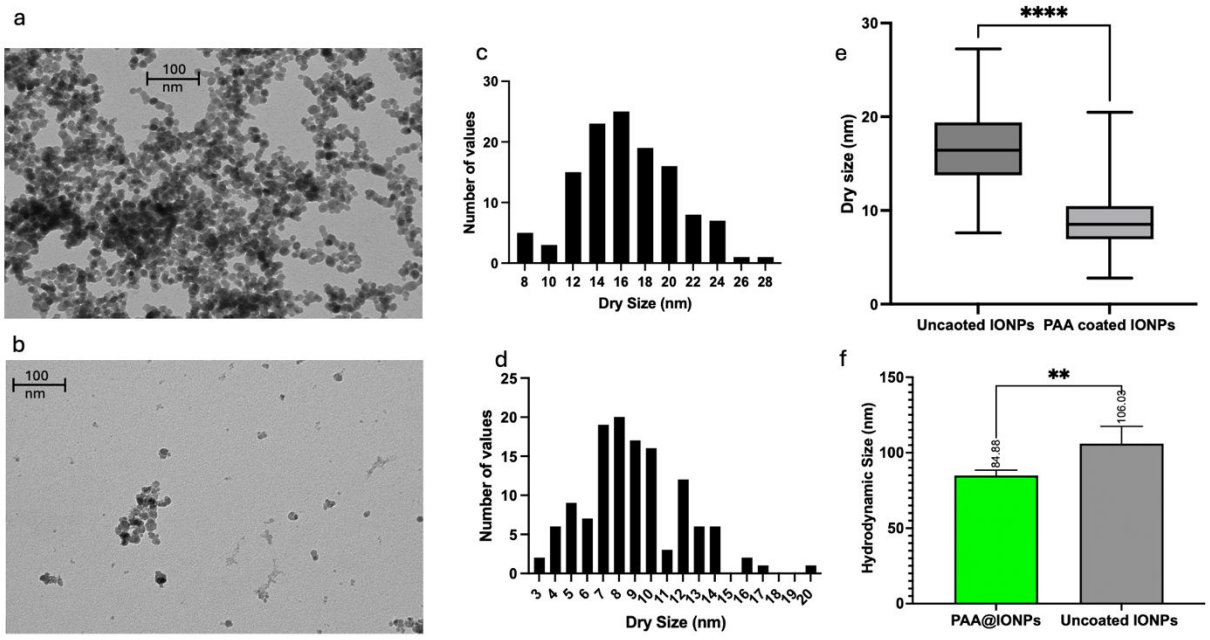

Figure 4 TEM images of synthesized (a) IONPs (magnification=60,000x) and (b) PAA@IONPs (magnification= 60,000x). All images were taken at an accelerating voltage of 80 kV. Dry size histogram of (c) IONPs, and (d) PAA@IONPs. (e) Comparison between dry size of IONPs and PAA@IONPs. **** $p < 0.0001$, n=127 f) Hydrodynamic size of IONPs and PAA@IONPs, determined by NTA. n = 5. ** p =0.0054

5- Hydrodynamic size smaller for PAA@IONPs than IONPs

When nanoparticles are dispersed in an aqueous solution, their surface properties and the ions present in the solution lead to the adsorption of molecules including but

not limited to water, ions, and proteins (if present in the solution) on their surface. This adsorption alters their size compared to their dry state, a phenomenon referred to as hydrodynamic size. To evaluate this size, we employed NTA. NTA measures the Brownian motion of individual nanoparticles using a combination of light microscopy and camera technology, providing a particle-by-particle analysis of size. This technique yields a detailed size distribution and allows for the clear visualization and differentiation of aggregates from single nanoparticles. As depicted in Figure 4f, the uncoated nanoparticles exhibited a significantly larger hydrodynamic size, averaging 106 ± 11 nm, compared to the coated nanoparticles, which averaged 84 ± 3 nm. This data underscores the influence of surface modifications on the hydrodynamic behavior of nanoparticles in solution. Our data also indicate that the hydrodynamic size of bare IONPs and PAA@IONPs increased by 6.75 ± 1.8 nm and 5.4 ± 0.7 nm, respectively, after the addition of nanoparticles to TSB. This increase might be attributed to the interaction with proteins and salts present in the TSB.

6- Coating enhanced colloidal stability of IONPs

PAA@IONPs demonstrated significantly higher colloidal stability compared to bare IONPs. After a week of storage, bare IONPs showed 60% absorbance loss due to sedimentation, while PAA@IONPs exhibited only a 22% decrease, indicating better particle suspension. Visual inspection confirmed less precipitation for PAA@IONPs, with lighter-colored solutions and sedimentation observed predominantly in bare IONPs. Additionally, zeta potential measurements showed significantly higher values for PAA@IONPs, indicating improved electrostatic stability due to the PAA coating. Further details and explanations of the results are provided in the supplementary materials.

7- Bacterial growth

7-1- Effect of hydrogen peroxide on bacterial growth is concentration-dependent

Hydrogen peroxide concentrations of 16 mM and below had minimal impact on bacterial growth, while concentrations above 400 mM completely inhibited it. To identify a concentration that reduced growth without eradicating bacteria, further testing revealed that a concentration of 182.25 mM caused approximately a 50% reduction in bacterial growth. This concentration was chosen for subsequent studies to assess the effect of coated and uncoated IONPs on bacterial growth inhibition in the presence of hydrogen peroxide. Additional explanations and related figures are provided in the supplementary file.

7-2- IONPs with hydrogen peroxide boost bacterial killing compared to IONPs alone

Figure 5a illustrates the impact of various concentrations of IONPs and PAA@IONPs on bacterial growth in the presence of 182.25 mM hydrogen peroxide. IONPs at concentrations higher than 1.825 mg/ml significantly increased bacterial growth inhibition while at lower concentrations the increase was not significant. PAA@IONPs did not have a significant impact on bacterial growth compared to the sample with just hydrogen peroxide. The concentration-dependent nature of these reactions for IONPs is evident in Figure 5a, showing that as the concentration of nanoparticles decreased, their effectiveness in inhibiting bacterial growth was also reduced. Having 3.65 mg/ml of IONPs and 182.25 mM of hydrogen peroxide resulted in decreases in bacterial growth of 91.57% and 65.83%, respectively, compared to the control sample and the one with hydrogen peroxide alone. Similarly, 3.65 mg/ml of PAA@IONPs reduced bacterial growth by 80.62% and 21.45% under the same conditions. The concentration dependence trend was not observed in PAA@IONPs samples. Figure 5-b compares the bacterial growth in presence of hydrogen peroxide between the same concentrations of IONPs and PAA@IONPs. IONPs inhibit bacterial growth more effectively than PAA@IONPs at the highest concentration.

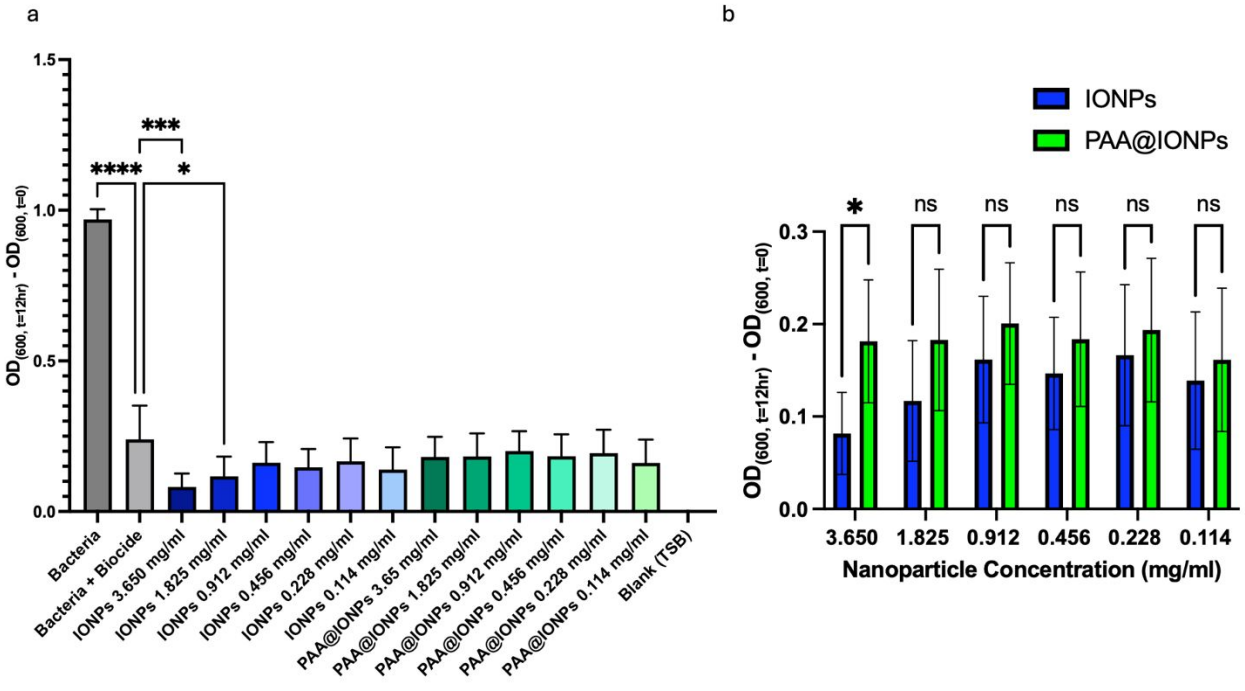

Figure 5 a) Impact of IONPs and PAA@IONPs with 182.25 mM of hydrogen peroxide on bacterial growth over 12 hr of incubation *p= 0.0296, *** p=0.0002, **** p<0.0001. n=6. b) Comparison of bacterial growth inhibition between IONPs and PAA@IONPs with 182.25 mM of hydrogen peroxide over 12 hr. *p= <0.0175, ns= not significant.

As a control to determine whether the nanoparticles themselves had antibacterial properties, the experiment above was repeated without hydrogen peroxide. As

shown in Figure 6, IONPs alone did not significantly affect bacterial growth over a 12 h incubation period. However, at the highest concentration (3.65 mg/ml), PAA-coated IONPs showed a slight reduction in bacterial growth. At lower concentrations, these changes were not statistically significant.

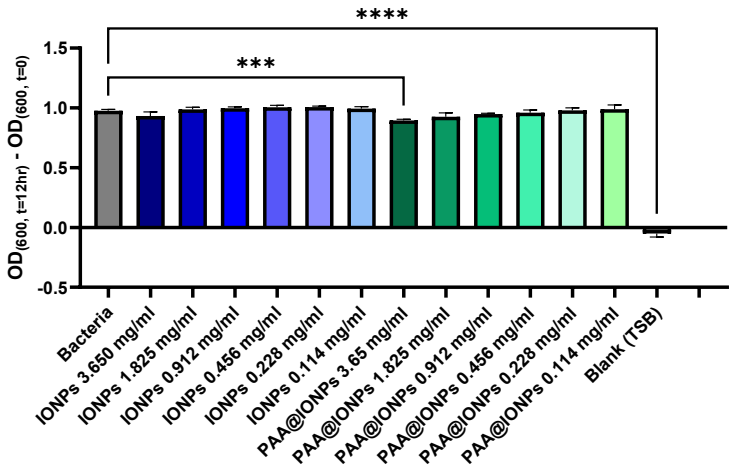

Figure 6 Impact of various concentrations of IONPs and PAA@IONPs on bacterial growth of *P. aeruginosa* after 12 hr of incubation *** p=0.0008, **** p<0.0001, n=3

7-3- IONPs have synergistic effect with hydrogen peroxide

Next, the concentration of nanoparticles was held constant while the concentration of hydrogen peroxide was varied by creating the following serial dilutions: 364.5, 182.25, 91.12, and 45.56 mM. Figure 7a shows the control samples, including both the bacteria and the blank. Figure 7b demonstrates that at the highest concentration, there was no bacterial growth in all samples, while at the lowest concentration, minimal growth inhibition was observed. When the concentration of hydrogen peroxide was set at 182.25 mM, the addition of IONPs significantly enhanced bacterial growth inhibition.

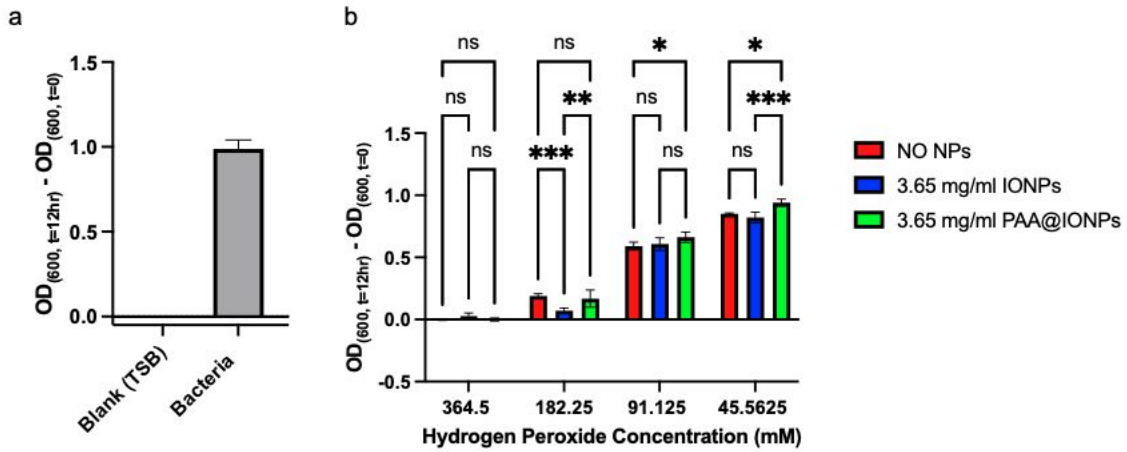

Figure 7 a) Growth of blank and bacteria as negative controls b) impact of various concentration of hydrogen peroxide with constant concentration of NPs on bacterial growth over 12 h. * p=0.0109, ** p=0.0059, *** p=0.0008, n=3

8- Antibacterial Study

The bar graph in Figure 8 presents the colony forming units (CFU) per 200 µL sample across various treatments against bacterial growth. The blank sample serves as a baseline with no countable colonies. In contrast, the sample with bacteria shows substantial growth with CFU reaching over 2 x 10^7, illustrating the bacteria growth under untreated conditions. When samples were treated with hydrogen peroxide, hydrogen peroxide along with IONPs, and hydrogen peroxide alongside PAA@IONPs, CFU dropped by 88.7, 90.2, and 89.6 %, respectively. As it is shown in Figure 8b, the sample with IONPs showed slightly more antibacterial activity but the statistical analysis showed that the difference was not significant.

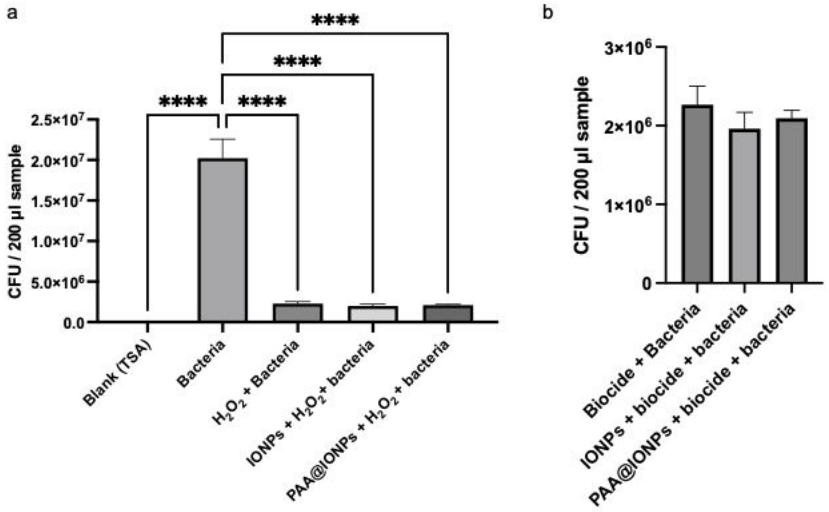

Figure 8 Number of colonies of *P. aeruginosa* that are formed after 15 h of incubation on the tryptic soy agar for (e) all samples (f) just H_2O_2+ Bacteria, IONPs+ H_2O_2+bacteria, and PAA@IONPs+H_2O_2+bacteria samples **** p<0.0001. n=3

10- pH Study:

The initial pH of TSB was 7.44 ± 0.03. Figure 9 illustrates the changes in pH for all samples after 12 h of incubation. Samples containing hydrogen peroxide exhibited a significant decrease in pH compared to the corresponding samples without H_2O_2. This pH reduction suggests the occurrence of a Fenton-like reaction, where hydrogen peroxide reacts with IONPs or PAA@IONPs, leading to the production of acidic species, which lowers the pH.

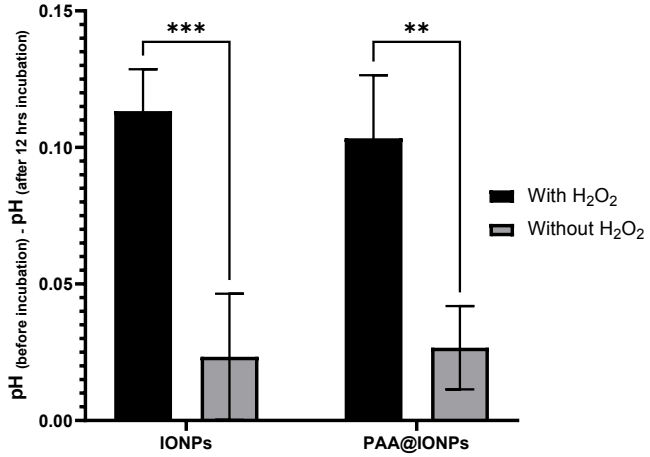

Figure 9 The changes of pH after incubation of IONPs and PAA@IONPs with and without hydrogen peroxide in TSB for 12 h. ** $p<0.0027$, *** $p<0.001$. n=3

Discussion:

Bacterial contamination in water systems poses significant challenges, including inhibited water flow, increased corrosion, and serious threats to human health [36]. Among the pathogens of concern, *P. aeruginosa* stands out due to its robustness and the health risks it presents. Traditional biocides used to control such bacteria often come with drawbacks, including potential harm to human health and the environment. In response to these challenges, this study explores an innovative approach to enhance the efficacy of hydrogen peroxide, a commonly used biocide. We hypothesize that IONPs could boost the antibacterial properties of hydrogen peroxide, offering a promising solution for improving water quality without the accompanying risks of increased chemical exposure.

The material properties of the particles synthesized for this study are shown in Figures 2-4. XRD data revealed six main peaks that are indicators of magnetic IONPs, and the PAA coating reduced the core IONP size. To determine whether the PAA coating on the IONPs was successful and if bonding occurred between the coating and the core, FTIR was conducted. Figure 10 illustrates the possible reactions between the coating and the core [29]. In reactions a and b, the C=O of PAA remains intact after coating, but in reactions c and d, the C=O bond of PAA breaks down. Our results showed that before coating, a high-intensity C=O peak was observed, and the peak intensity significantly dropped after coating, indicating that bonding between PAA and IONPs occurred and it was either in form c or d (Figure 10). Same trend was also seen in XPS results (Figure 1 in supplementary file). Additionally, the intensity of the Fe-O peak in the coated sample decreased compared to the bare IONPs, likely due to the surface coverage of the IONPs by the coating.

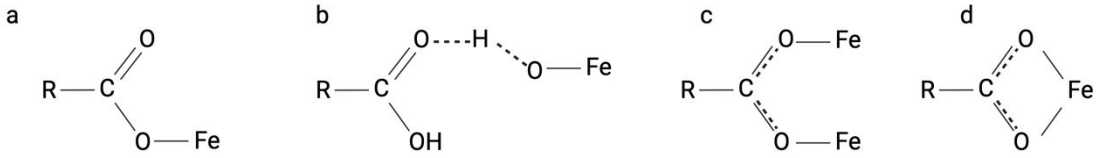

Figure 10 possible interactions of the PAA polymer chain and IONPs.

To achieve optimal activity in the Fenton and Fenton-like reactions, the IONPs needed to be in the magnetite oxidation state. Zhao et al. [37] reported that magnetite nanoparticles show stronger catalytic performance compared to hematite, and hydrated iron(III) oxide in Fenton reactions. The XPS technique confirmed that the synthesized nanoparticles were indeed magnetite. This analysis also indicated that the drying technique significantly affects the oxidation state of the final product.

The TEM analysis revealed that the inclusion of PAA during synthesis to coat the particles significantly influenced the size of the IONPs, reducing the mean particle size from 16 ± 3 nm for uncoated to 9 ± 2 nm for coated nanoparticles. The observed differences in hydrodynamic sizes between coated and uncoated nanoparticles measured by NTA aligned well with TEM images, highlighting the coating's effectiveness in inhibiting particle agglomeration and promoting IONPs uniformity.

Hydrodynamic size of PAA@IONPs were 22 nm smaller than bare IONPs. The reason that the addition of a polymer coating resulted in a decrease in hydrodynamic size rather than an increase is that the PAA coating was introduced before nucleation and formation of IONPs. As the nanoparticles formed, they were immediately coated with PAA, which prevented aggregation and further growth, ultimately leading to the formation of smaller nanoparticles. Smaller nanoparticles have a higher surface area-to-volume ratio, which enhances their interaction with the surrounding medium and promotes better electrostatic stabilization [38, 39]. The UV-vis absorbance at 350 nm showed that PAA@IONPs exhibited smaller changes in peak intensity compared to bare IONPs, indicating better stability in an aqueous environment. Sedimentation studies further supported this, as PAA@IONPs demonstrated decreased sedimentation rates, reflecting their increased colloidal stability. Additionally, zeta potential measurements revealed that PAA@IONPs had more negative values, suggesting stronger repulsive forces between particles and thereby enhancing stability. Improved colloidal stability means that nanoparticles are less likely to aggregate and precipitate, which is critical for maintaining consistent interaction with hydrogen peroxide to enhance antibacterial activity, leading to more effective performance in water treatment.

In this study, we aimed to enhance the efficacy of hydrogen peroxide by leveraging IONPs through the Fenton and Fenton-like reactions. This approach was expected to lower the required concentrations of hydrogen peroxide. The impact of hydrogen peroxide on bacterial growth is highlighted in Figure 4 in the supplementary file, where lower concentrations (0.5 to 16 mM) did not significantly affect growth, but levels above 81 mM markedly reduced it, with a 50% reduction observed at 182.25 mM, which is the concentration chosen for further studies. Figure 5 then compares the bacterial growth inhibition of uncoated IONPs and PAA@IONPs in the presence of hydrogen peroxide. It shows that bare IONPs at concentrations higher than 1.825 mg/ml, significantly reduced bacterial growth compared to the control without nanoparticles. Although other samples exhibited increased bacterial inhibition, their impacts were not statistically significant. This could be because the bare surface of IONPs provides more active sites for catalyzing the Fenton and Fenton-like reactions compared to PAA-coated IONPs, where the polymer coating may hinder access to the iron cores necessary for the reaction. The lack of significant increase in bacterial inhibition at lower IONPs concentrations, indicated that the reactions were concentration-dependent, with a minimum effective concentration of 1.825 mg/ml needed to observe a notable effect.
Figure 9 illustrates a decrease in pH to a more acidic environment following the incubation of nanoparticles with hydrogen peroxide, indicative of Fenton and Fenton-like reactions.

Despite existing literature suggesting that neither IONPs nor PAA exhibits substantial antibacterial activity [17, 40], Nie et al. [20] have indicated that coating IONPs with PAA enhanced their bactericidal effects against *Escherichia coli* and *Staphylococcus aureus*. Nonetheless, our findings did not reveal a significant impact of the PAA@IONPs alone on *P. aeruginosa*. The bacterial inhibition studies (Figure 6) indicated that at the highest concentrations, PAA-coated IONPs could slightly inhibit bacterial growth compared to uncoated IONPs, while at lower concentrations, neither type of nanoparticle displayed substantial activity in the absence of hydrogen peroxide. This outcome supports the hypothesis that the bacterial growth inhibition observed in the previous experiment involving hydrogen peroxide was primarily due to the Fenton and Fenton-like reactions between ferrous and ferric iron and hydrogen peroxide molecules.

Figure 7b illustrates that there was a specific concentration range of hydrogen peroxide within which the addition of IONPs could significantly enhance bacterial growth inhibition via the Fenton and Fenton-like reactions. At high concentrations, hydrogen peroxide alone was sufficient to inhibit bacterial growth, while at low concentrations, the generation of radical ROS through the Fenton and Fenton-like

reactions was inadequate to effectively inhibit bacterial growth. In our study, the addition of IONPs in the presence of 182.25 mM hydrogen peroxide notably increased their efficacy in inhibiting bacterial growth. Combining Figure5-7, it is evident that IONPs alone do not affect bacterial growth. However, when combined with hydrogen peroxide, they significantly inhibit bacterial growth, and this effect intensifies at the optimum concentration of hydrogen peroxide (182.25 mM). This indicates that the impact of IONPs and hydrogen peroxide on bacterial growth inhibition is synergistic, not additive.

The absence of bacterial colonies in the blank samples (Figure 8) confirmed that our experiments were not contaminated. Bacteria samples exhibited significantly higher colony numbers compared to other samples, indicating optimal conditions for bacterial growth. Samples treated with H_2O_2 showed significantly lower CFU compared to the bacteria-only samples, suggesting effective bacterial cell eradication. Although our previous data indicated that the presence of IONPs could enhance the bacterial inhibition growth effects of biocides by triggering the Fenton and Fenton-like reactions, the CFU counts in the samples with IONPs were lower than those without, but the difference was not statistically significant. PAA-coated IONPs showed antibacterial activity slightly lower than samples with uncoated IONPs and slightly higher than the samples without nanoparticles but the differences were not statistically significant.

Our data showed that the presence of IONPs can enhance the effectiveness of hydrogen peroxide. The literature reports that 294 mM of hydrogen peroxide effectively kills *Escherichia coli* in 75 min and *Streptococcus faecalis* in 180 min [41]. With the aid of IONPs, we achieved a 90.2% kill rate of *P. aeruginosa* in 60 min. Although coatings can improve the storage stability and decrease the size of nanoparticles, the presence of polymer chains hindered the catalytic activity of IONPs with hydrogen peroxide. Future studies should investigate the impact of coating coverage on the colloidal stability and reactivity of IONPs in the Fenton reaction. Identifying the optimal coverage of IONPs that enhances their colloidal stability while maintaining their reactivity in the Fenton reaction could significantly benefit the water treatment industry. Our study was limited to *P. aeruginosa*, while future research should include other bacterial strains to draw more definitive conclusions. The application of alternating magnetic fields to induce hyperthermia in these nanoparticles will be explored by our team, which could further reduce the required biocide concentrations for effective bacterial eradication.

Conclusions:

This study attempted to find a solution to decrease the concentration of hydrogen peroxide necessary to limit bacterial growth in water sources. In this study, bare IONPs combined with hydrogen peroxide were effective against bacterial growth at concentrations higher than 1.825 mg/ml. PAA@IONPs combined with hydrogen peroxide were more effective than hydrogen peroxide alone, however, the difference was not statistically significant. Although coating the IONPs with PAA decreased the size of the nanoparticles and increased their colloidal stability, it also reduced their ability to inhibit bacterial growth. This reduction is most likely due to the smaller effective surface area available for Fenton and Fenton-like reactions to occur on the iron surface. This strategy holds promise for mitigating the spread of infectious diseases in diverse settings, ranging from hospital water systems to industrial applications and even space station water recovery systems.

Acknowledgments:
This work was supported by National Aeronautics and Space Administration (NASA) Grant 80NSSC21M0325. The authors thank the Harry Hood Bassett Flow Cytometry and Small Particles Detection (FCSPD) Facility for access to the NTA instrument, which was obtained by NIH grant S10-OD002976. Also, the authors thank the UVM Microscopy Imaging Center for the use of the JEOL 1440 TEM. The authors also extend their gratitude to Dr. Nicolas Perdrial for providing access to XRD analysis. They also thank Eli Borin, an undergraduate student who helped with the synthesize of a few preliminary batches of nanoparticles.

References:

1. Organization, W.H. *Drinking-water*. 2023; Available from: https://who.int/news-room/fact-sheets/detail/drinking-water#:~:text=Microbiologically%20contaminated%20drinking%20water%20can,food%20production%20or%20recreational%20purposes.
2. Mena, K.D. and C.P. Gerba, *Risk assessment of Pseudomonas aeruginosa in water.* Reviews of environmental contamination and toxicology Vol 201, 2009: p. 71-115.
3. Loveday, H., et al., *Association between healthcare water systems and Pseudomonas aeruginosa infections: a rapid systematic review.* Journal of Hospital Infection, 2014. **86**(1): p. 7-15.
4. Qin, S., et al., *Pseudomonas aeruginosa: pathogenesis, virulence factors, antibiotic resistance, interaction with host, technology advances and*

emerging therapeutics. Signal transduction and targeted therapy, 2022. **7**(1): p. 199.
5. Maillard, J.-Y., *Antimicrobial biocides in the healthcare environment: efficacy, usage, policies, and perceived problems.* Therapeutics and clinical risk management, 2005. **1**(4): p. 307-320.
6. Cabiscol Catalā, E., J. Tamarit Sumalla, and J. Ros Salvador, *Oxidative stress in bacteria and protein damage by reactive oxygen species.* 2000.
7. Jones, I.A. and L.T. Joshi, *Biocide use in the antimicrobial era: a review.* Molecules, 2021. **26**(8): p. 2276.
8. Watt, B.E., A.T. Proudfoot, and J.A. Vale, *Hydrogen peroxide poisoning.* Toxicological reviews, 2004. **23**: p. 51-57.
9. Nelson, A.L. and L. Porter, *Hydrogen peroxide toxicity.* 2022.
10. Wu, H., et al., *Reactive oxygen species-related activities of nano-iron metal and nano-iron oxides.* Journal of Food and Drug Analysis, 2014. **22**(1): p. 86-94.
11. Ranji-Burachaloo, H., et al., *Cancer treatment through nanoparticle-facilitated fenton reaction.* ACS nano, 2018. **12**(12): p. 11819-11837.
12. Suman, S., et al., *Biotic stresses on plants: reactive oxygen species generation and antioxidant mechanism*, in *Frontiers in plant-soil interaction*. 2021, Elsevier. p. 381-411.
13. Kobayashi, Y., et al., *Bactericidal effect of hydroxyl radicals generated from a low concentration hydrogen peroxide with ultrasound in endodontic treatment.* Journal of clinical biochemistry and nutrition, 2014. **54**(3): p. 161-165.
14. Nguyen, T.-K., et al., *Iron oxide nanoparticle-mediated hyperthermia stimulates dispersal in bacterial biofilms and enhances antibiotic efficacy.* Scientific reports, 2015. **5**(1): p. 18385.
15. Patil, S.A., et al., *Manganese Iron Oxide Nanoparticles for Magnetic Hyperthermia, Antibacterial and ROS Generation Performance.* Journal of Cluster Science, 2024. **35**(5): p. 1405-1415.
16. Kotrange, H., et al., *Metal and metal oxide nanoparticle as a novel antibiotic carrier for the direct delivery of antibiotics.* International Journal of Molecular Sciences, 2021. **22**(17): p. 9596.
17. Borcherding, J., et al., *Iron oxide nanoparticles induce Pseudomonas aeruginosa growth, induce biofilm formation, and inhibit antimicrobial peptide function.* Environmental Science: Nano, 2014. **1**(2): p. 123-132.
18. Ramezani Ali Akbari, K. and A. Abdi Ali, *Study of antimicrobial effects of several antibiotics and iron oxide nanoparticles on biofilm producing pseudomonas aeruginosa.* Nanomedicine Journal, 2017. **4**(1): p. 37-43.

19. Martemucci, G., et al., *Free radical properties, source and targets, antioxidant consumption and health.* Oxygen, 2022. **2**(2): p. 48-78.
20. Nie, L., et al., *Poly (acrylic acid) capped iron oxide nanoparticles via ligand exchange with antibacterial properties for biofilm applications.* Colloids and Surfaces B: Biointerfaces, 2021. **197**: p. 111385.
21. Cao, C., et al., *Recent advances of cancer chemodynamic therapy based on Fenton/Fenton-like chemistry.* Chemical science, 2022. **13**(4): p. 863-889.
22. Jiang, C., et al., *A new insight into Fenton and Fenton-like processes for water treatment.* Journal of hazardous materials, 2010. **174**(1-3): p. 813-817.
23. Nelson, A.L. and L. Porter, *Hydrogen Peroxide Toxicity*, in *StatPearls*. 2025, StatPearls Publishing

24. Nwasike, C., et al., *Activatable superparamagnetic iron oxide nanoparticles scavenge reactive oxygen species in macrophages and endothelial cells.* RSC advances, 2020. **10**(68): p. 41305-41314.
25. Yoo, E., et al., *Activatable interpolymer complex-superparamagnetic iron oxide nanoparticles as magnetic resonance contrast agents sensitive to oxidative stress.* Colloids and Surfaces B: Biointerfaces, 2017. **158**: p. 578-588.
26. Paige, S., et al., *The impact of ammonium hydroxide flow rate on iron oxide nanoparticle hydrodynamic size and colloidal stability.* Colloids and Surfaces A: Physicochemical and Engineering Aspects, 2024: p. 135018.
27. Iyengar, S.J., et al., *Magnetic, X-ray and Mössbauer studies on magnetite/maghemite core–shell nanostructures fabricated through an aqueous route.* RSC advances, 2014. **4**(110): p. 64919-64929.
28. He, Q., et al., *Chemically surface tunable solubility parameter for controllable drug delivery—An example and perspective from hollow PAA-coated magnetite nanoparticles with R6G model drug.* Materials, 2018. **11**(2): p. 247.
29. Sanchez, L.M., et al., *Polyacrylic acid-coated iron oxide magnetic nanoparticles: The polymer molecular weight influence.* Colloids and Surfaces A: Physicochemical and Engineering Aspects, 2018. **543**: p. 28-37.
30. Zhou, C., et al., *Synthesis of poly (acrylic acid) coated-Fe3O4 superparamagnetic nano-composites and their fast removal of dye from aqueous solution.* Journal of Nanoscience and Nanotechnology, 2013. **13**(7): p. 4627-4633.
31. Xu, Y., et al., *Bleomycin loaded magnetite nanoparticles functionalized by polyacrylic acid as a new antitumoral drug delivery system.* BioMed Research International, 2013. **2013**(1): p. 462589.

32. Lu, J., et al., *Solvothermal synthesis and characterization of Fe3O4 and γ-Fe2O3 nanoplates.* The Journal of Physical Chemistry C, 2009. **113**(10): p. 4012-4017.
33. Kolen'ko, Y.V., et al., *Large-scale synthesis of colloidal Fe3O4 nanoparticles exhibiting high heating efficiency in magnetic hyperthermia.* The Journal of Physical Chemistry C, 2014. **118**(16): p. 8691-8701.
34. Wang, J., et al., *A platinum anticancer theranostic agent with magnetic targeting potential derived from maghemite nanoparticles.* Chemical Science, 2013. **4**(6): p. 2605-2612.
35. Gao, Q., et al., *The study of novel Fe3O4@ γ-Fe2O3 core/shell nanomaterials with improved properties.* Journal of magnetism and magnetic materials, 2009. **321**(8): p. 1052-1057.
36. Liu, S., et al., *Understanding, monitoring, and controlling biofilm growth in drinking water distribution systems.* Environmental science & technology, 2016. **50**(17): p. 8954-8976.
37. Zhao, L., et al., *Catalytic activity of different iron oxides: Insight from pollutant degradation and hydroxyl radical formation in heterogeneous Fenton-like systems.* Chemical Engineering Journal, 2018. **352**: p. 343-351.
38. Austin, J., et al., *Nanoparticle number concentration measurements by multi-angle dynamic light scattering.* Journal of Nanoparticle Research, 2020. **22**(5): p. 108.
39. Abbas, Z., et al., *Size-dependent surface charging of nanoparticles.* The Journal of Physical Chemistry C, 2008. **112**(15): p. 5715-5723.
40. Ni, Z., et al., *Synthesis of poly acrylic acid modified silver nanoparticles and their antimicrobial activities.* Materials Science and Engineering: C, 2014. **41**: p. 249-254.
41. BAYLISS, C.E. and W. Waites, *The effect of hydrogen peroxide and ultraviolet irradiation on non-sporing bacteria.* Journal of Applied Microbiology, 1980. **48**(3): p. 417-422.

Data for this article, including figures and their raw data are available at NOMAD at https://nomad-lab.eu/prod/v1/gui/user/uploads/upload/id/U6a79B7wRaaoayclWomN-g